REMARKS

Claims 1 and 4-6 are pending in the application and are rejected.

The Examiner has finally rejected claims claims 1 and 4-6 under 35 USC 103(a) as being unpatentable over Smith (6,187,213) in view of Weir (6,710,943) for the reasons set forth in Paragraph 3 of the Official Action. The Smith reference discloses a gemstone having a micro-discrete indicia formed using convention optics. The Examiner has acknowledged that the Smith reference does not expressly state the use of near-field optics. The Examiner argues that the process limitation has not been given any patentable weight if it is the same or obvious product of the prior art. In this regard, Applicant respectfully submits that the product made according to the present invention is not the same as cited in the prior art. In the prior art Smith reference, indicia is formed using conventional optics to form an indicia. However, this does not and cannot form the same product to which the present invention is directed. Accordingly it is respectfully submitted that the process limitation is to be given patentable weight. Near-field optical systems such as that set forth in the present invention provides significant advantages over conventional optical systems as disclosed in the cited art. The resolution of an optical system determines the lower limit on both the reading and writing processes.

Enclosed herewith is an article entitled Micromachines Silicon Nitride Solid Immersion Lens. As can be seen from the attached article a significant resolution improvement is obtained through the use of solid immersion lenses. In particular the improvement for a particular lens material is 1.98 over conventional optical systems. So called tapered optical fiber near-field optical systems offer the potential of even greater resolution improvement (approximately 100 x) over conventional designs but at the sacrifice of reduced optical through put . Regardless of the near-field optical system embodiment used, the near-field optical system of the present invention offers the advantage of creating indicia that is unreadable, is unwriteable by conventional optical systems as the resolution improvement is not provided by the prior art. This sets forth in the present invention that micro-discrete indicia image has a length no greater than 10 microns and a height no greater than 2 microns. This is illustrated by reference to figure 4. The cited prior art totally fails to teach or suggest the

capability of providing such small indicia. As set forth in the present invention it is the entire indicia , i.e. the plurality and members that have a height and length dimension. Thus it more than simply a mark it is a whole indicia that provides a plurality of information and not simply a tiny mark. Thus, it is respectfully submitted that the difference provided through the use of a near-field optics provides a totally apart and distinct article form the cited art. Furthermore there is no reaching or suggestion in any of the references cited for using near field optics in crating indicia optics and creating indicia of the size and type claimed by application.

In view of the foregoing it is respectfully submitted that the claims in their present form are in condition for allowance and such action is respectfully requested.

The Commissioner is hereby authorized to charge any fees in connection with this communication to Deposit Account No. 05-0225.

Respectfully submitted,

Attorney for Applicant(s)
Registration No. 27,370

Frank Pincelli/phw
Rochester, NY 14650
Telephone: 585-722-3335
Facsimile: 585-477-4646
If the Examiner is unable to reach the Applicant(s) Attorney at the telephone number provided, the Examiner is requested to communicate with Eastman Kodak Company Patent Operations at (585) 477-4656.

Micromachined Silicon Nitride Solid Immersion Lens

Kenneth B. Crozier, *Student Member, IEEE*, Daniel A. Fletcher, Gordon S. Kino, *Life Fellow, IEEE*, and Calvin F. Quate, *Life Fellow, IEEE*

Abstract—We present a fabrication method for silicon nitride solid immersion lenses (SILs) integrated with atomic force microscope (AFM) cantilevers. We demonstrate a scanning optical microscope based on the microfabricated SIL that operates in reflection and transmission modes at a wavelength of $\lambda = 400$ nm. In this microscope, light is focused to a spot in a high refractive index SIL held close to the sample. The minimum spot size of a SIL-based microscope, which determines the transverse optical resolution, is $\lambda/(2n)$ where n is the refractive index of the SIL. This is smaller than the minimum spot size of $\lambda/2$ in air. The SIL, therefore, makes possible optical resolution better than the diffraction limit in air. The full-width at half-maximum (FWHM) spot size of the SIL-based microscope is measured to be ~133 nm in transmission mode, which is ~1.98 times better than the spot size measured without the SIL (264 nm). This improvement factor is close to the refractive index of the silicon nitride SIL ($n = 1.96$). [797]

Index Terms—Atomic force microscopy (AFM), microlens, near-field scanning optical microscopy, scanning probe microscopy, solid immersion lens (SILs).

Fig. 1. Solid immersion microscopy with micromachined SIL integrated onto an AFM cantilever. The effective numerical aperture is $NA_{eff} = n \sin \theta$. In this work, $NA_{eff} = 1.57$. Light is focused to a spot at the end of the tip and the sample is scanned.

I. INTRODUCTION

DUE TO diffraction, light cannot be focused to an arbitrarily small spot even by a perfect lens free from aberrations. The full-width at half-maximum (FWHM) spot size, which determines the transverse spatial resolution of an optical system, is given in the paraxial approximation by $\sim \lambda/(2NA)$, where λ is the wavelength and NA is the numerical aperture. NA is equal to $n \sin \theta$, where n is the refractive index at the focal point and θ is the illumination half angle. In a standard optical microscope operating in air, the maximum value of NA is 1.0 and the minimum spot size is therefore $\lambda/2$. In solid immersion microscopy [1], light is focused to a spot in a high-refractive index lens held close to the sample. The maximum value of NA is increased to n, the refractive index of the SIL. Because the minimum spot size is then $\lambda/(2n)$, the transverse optical resolution is improved by a factor of n. This is illustrated in Fig. 1, which shows a solid immersion microscope based on a micromachined SIL integrated on an atomic force microscope (AFM) cantilever. Light is focused by a lens into the SIL to form a spot at the end of the tip and reflected and transmitted by the sample. The image of the sample is built up by recording the reflection and transmission intensities as the sample is scanned.
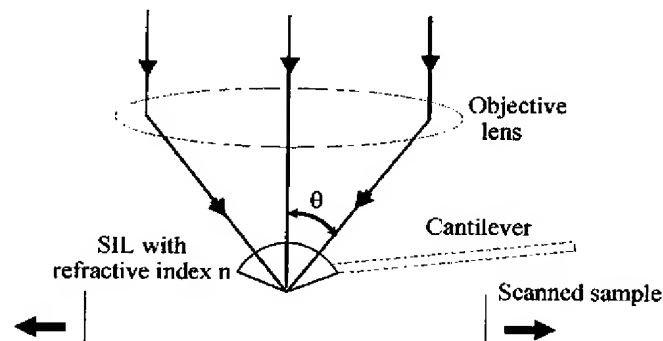
The SIL has near unity optical throughput, limited only by reflections from its surfaces (which may be reduced by antireflection coatings) and by absorption losses in the SIL (which are small if the SIL material is chosen appropriately). Optical resolution well below the diffraction limit in air is possible with the SIL. For example, a gallium phosphide SIL at a wavelength of $\lambda = 544$ nm (where $n = 3.463$ [2]) has a theoretical spot size of $\sim \lambda/(2n) \sim 79$ nm. At a wavelength of $\lambda = 155$ nm (where $n = 1.702$ [2]), a silicon dioxide SIL has a theoretical spot size of $\sim \lambda/(2n) \sim 46$ nm. At these wavelengths, the optical losses through 3.1 μm radius SILs of both materials are less than 1% [2]. The SIL has better optical throughput efficiency than the tapered fiber nearfield scanning optical microscope (NSOM) [3], an alternative approach for improving optical resolution below the diffraction limit in air. The typical light throughput efficiency of a conventional tapered optical fiber is poor, about 10^{-5} for a 100 nm diameter aperture at a wavelength of $\lambda = 633$ nm [4], though recent work in double and triple tapered optical fibers has improved this to $\sim 4 \times 10^{-3}$ [5]. The micromachined SIL has the further advantage that the SILs may be made in closely spaced arrays, allowing imaging of the sample through multiple SILs simultaneously, leading to an improvement in imaging speed.

Most previous versions of the SIL (e.g., [1]) were made using conventional lens making techniques and therefore had diameters of ~ 1 mm or greater. With micromachining, it is possible to fabricate a SIL with a diameter of less than 10 μm. This allows the SIL to be fabricated onto a thin (< 1 μm), compliant cantilever with a high resonant frequency (69 kHz in this work) to enable fast scanning and a low spring constant (to minimize tip-sample forces). We have previously demonstrated infrared applications of silicon SILs made using micromachining [6]. Microscopy at visible wavelengths ($\lambda = 633$ nm) has also been

demonstrated using these SILs [7], although absorption of the light in the silicon led to optical transmission through the SIL being only ~3%. In this work, the SIL is fabricated from silicon nitride, allowing for high optical transmission efficiency at the visible and UV wavelengths used in microscopy, data storage and lithography.

In this paper we present the theory, fabrication and testing of silicon nitride solid immersion lenses (SILs) integrated with AFM cantilevers. In Section II, the theory of the SIL is reviewed. In Section III, a surface micromachining fabrication method for silicon nitride SILs is described. The edge response of the SIL microscope, the point spread function and images taken with it, demonstrating the improved optical resolution available with the SIL, are presented in Section IV.

II. THEORY

The simplest form of the SIL, known as the hemispherical SIL, is illustrated in Fig. 1. The curved surface of the SIL is spherical, with the center of curvature located at the focal point of the lens used to focus the light into the SIL. Light rays therefore enter the SIL along radii and converge at its center. In this configuration, the SIL does not focus the incoming light rays. Rather, it provides a high refractive index medium in which the light may be focused to a smaller spot than in air. In this section, the transverse optical resolution of the SIL microscope in transmission and reflection modes is calculated.

A. Transverse Optical Resolution

The transverse spatial resolution of the SIL microscope is determined by its point spread function (PSF). In the paraxial approximation, the amplitude PSF $h(r)$ is given by an Airy function [8]

$$h(r) = \frac{2J_1(kr\sin\theta)}{kr\sin\theta} \qquad (1)$$

where J_1 is a Bessel function of the first kind, order 1, r is the radial position, θ is the illumination half angle and $k = 2\pi n/\lambda$ where n is the refractive index of the SIL and λ the illumination wavelength.

It may be shown [8] that for a confocal microscope with point source illumination and point detection, the intensity signal at the detector is given by ·

$$I = \left|h^2 * s\right|^2 \qquad (2)$$

where $*$ represents convolution and s is the sample amplitude response. Therefore, the image obtained by a confocal microscope is the square of the convolution of the intensity PSF (h^2) with the amplitude response of the sample s. We expect to obtain these imaging characteristics with the SIL microscope operating in reflection mode, since we use a pinhole to obtain point illumination and detection.

It may also be shown [8] that for a microscope with a coherent focused input beam and a large area detector the intensity signal is given by

$$I = |h * s|^2. \qquad (3)$$
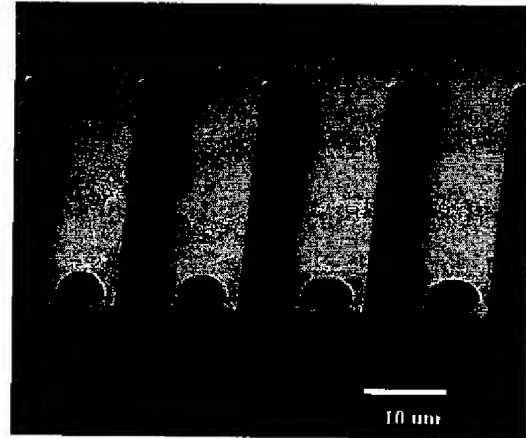
(a)
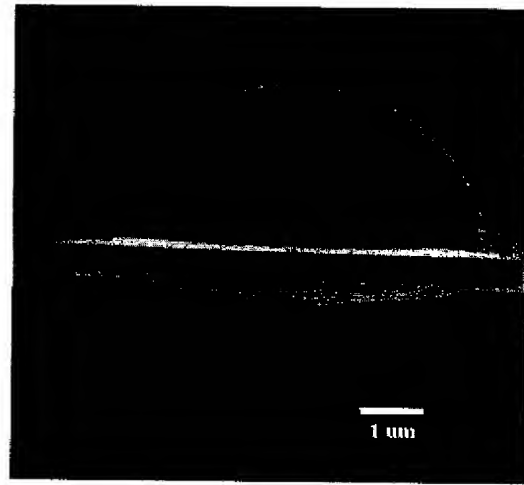
(b)

Fig. 2. (a) SEM showing silicon nitride SILs on cantilevers. There is a tip opposite each SIL. Cantilever dimensions: $L = 92\,\mu\mathrm{m}$, $W = 10\,\mu\mathrm{m}$, $T = 0.5\,\mu\mathrm{m}$. (b) Close-up SEM of SIL. SIL radius $= 3.1\,\mu\mathrm{m}$, cantilever thickness $T = 0.5\,\mu\mathrm{m}$ and tip height is $0.5\,\mu\mathrm{m}$.

This assumes that the illumination is perfectly coherent, so the electric field amplitudes (E) add at the detector. For incoherent illumination, the electric field intensities (E^2) add at the detector and the detector intensity signal is given by

$$I = |h|^2 * |s|^2. \qquad (4)$$

As will be discussed in Section IV, the illumination in the SIL microscope built for this study may be considered incoherent and the transmission mode imaging characteristics are therefore given by (4).

While the amplitude PSF $h(r)$ given by the paraxial approximation is accurate enough for most purposes, the exact form of the PSF $h(r)$ may be calculated using vector diffraction theory [9]. Using vector diffraction theory, we calculate the FWHM spot size of the intensity PSF h^2 to be 256 nm without the SIL and 130 nm with the SIL. These calculations assume that the illumination is $\lambda = 400$ nm, that the numerical aperture NA of the objective lens is 0.8 and that the SIL has a refractive index
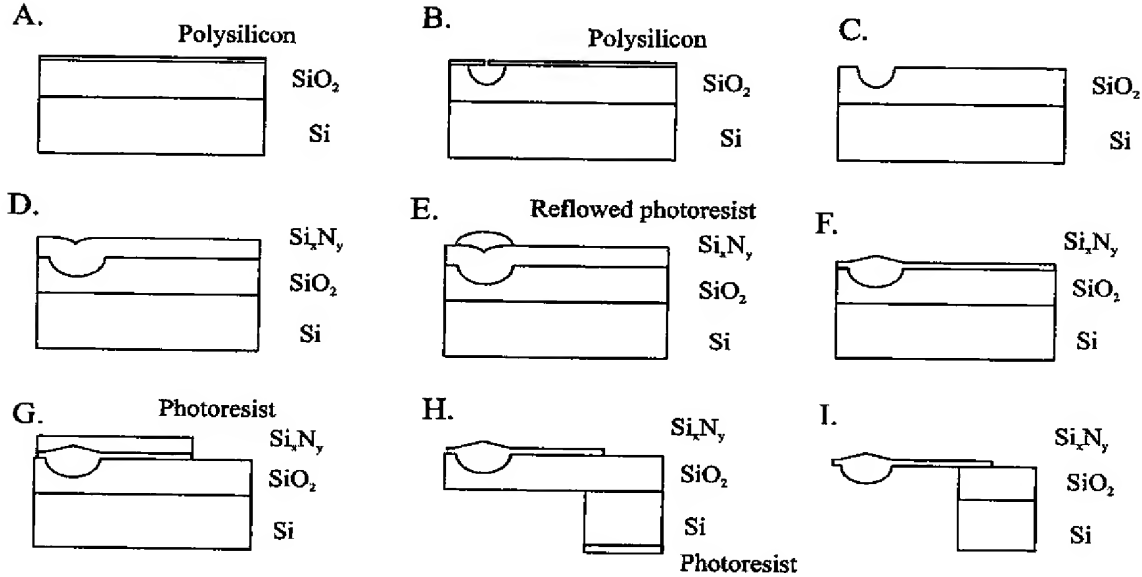
Fig. 3. Fabrication process for silicon nitride SILs.

of 1.96. The SIL reduces the width of the intensity PSF by 1.96 and improves the transverse spatial resolution.

B. Tolerances in SIL Dimensions

A major advantage of using small micromachined SILs is that, because of their small size, aberration due to errors in the radius or thickness of the lens are very small. Hence tolerances in micromachining the lenses are relatively large.

The allowable tolerance Δz in the thickness of the SIL for a wave aberration Φ, where a is the SIL radius, n is the refractive index and $\sin \theta_0$ is the objective lens $N.A.$ is [10]

$$\Delta z = \sqrt{\frac{8a\Phi}{n(n-1)\sin^4 \theta}}. \tag{5}$$

Taking a wave aberration of $\Phi = \lambda/4$ (which should have a minimal effect on the transverse resolution [10]) the thickness tolerance Δz is found to be ~ 1.8 μm for a SIL of radius $a = 3.1$ μm, with $\lambda = 400$ nm, $n = 1.96$ and $\sin \theta_0 = 0.8$. Clearly, this is a fairly easy tolerance to meet, as it is equivalent to $\sim 58\%$ of the SIL radius. By contrast, a 1 mm-radius SIL with the same parameters has $\Delta z = 32 \mu$m, which is only $\sim 3\%$ of the SIL radius. Therefore, as the SIL is made smaller, the relative height tolerance improves.

III. FABRICATION

A scanning electron micrograph (SEM) of a linear array of silicon nitride SILs fabricated on AFM cantilevers with a tip opposite each SIL is shown as Fig. 2(a). The cantilever is 92 μm long and 10 μm wide. From Fig. 2(b), a close-up SEM of the SIL and tip, it may be seen that the cantilever has a thickness of 0.5 μm and the tip height is 0.5 μm. Unlike a sharp AFM tip, the SIL tip is designed to be fairly blunt so that its half angle (71°) exceeds or matches the acceptance angle θ of the focusing lens (53°). From Fig. 2(b), the curved surface of the SIL may be fitted

to a sphere of radius $a = 3.1$ μm, with deviations of the actual SIL surface from this sphere being less than ~ 80 nm. The center of the sphere is ~ 0.8 μm above the end of the tip and this may be taken to be the error in the height of the SIL. From this, the expected wave aberration calculated from (5) is $\sim \lambda/19$, which should have a negligible effect upon the PSF. It is also expected that the deviations of the surface from spherical (<80 nm) and the surface roughness (RMS < 20 nm) will have little effect upon the PSF.

A. Fabrication Process

The fabrication process is shown in Fig. 3. The fabrication process and preliminary testing results (with an HeNe laser at $\lambda = 633$ nm) were previously reported in [11]. Silicon dioxide (SiO_2, 4.5 μm thick) and polysilicon (0.3 μm thick) films are deposited on the silicon wafer by low-pressure chemical vapor deposition (LPCVD, step A). Holes (1 μm diameter) are then plasma etched (HBr : O_2) in the polysilicon. Hemispherical cavities (3–3.5 μm radius) are wet etched in the SiO_2 using hydrofluoric acid (6 : 1 buffered oxide etch—BOE) through the holes in the polysilicon (step B). Fig. 4(a) is an SEM of cavities etched into SiO_2. The hemispherical shape of the cavities is illustrated in the cross-section SEM of Fig. 4(b). After plasma etching (HBr : O_2) the polysilicon to remove it (step C), 6.8 μm of silicon nitride (Si_xN_y) is deposited by dual-frequency plasma enhanced chemical vapor deposition (PECVD, step D). Pillars of photoresist (~ 1.5 μm height) are patterned by lithography and reflowed thermally in a 150 °C oven for 16 min (step E). The photoresist height is then measured by AFM and plasma etching (O_2) is used to reduce the photoresist height. This height and the relative etch rates of silicon nitride and photoresist in the subsequent etch step determine the final silicon nitride tip height, which should be at the focal point of the SIL. Plasma etching ($CHF_3 : O_2$) is then used to transfer the photoresist shape into the underlying silicon nitride, resulting in a tip opposite the
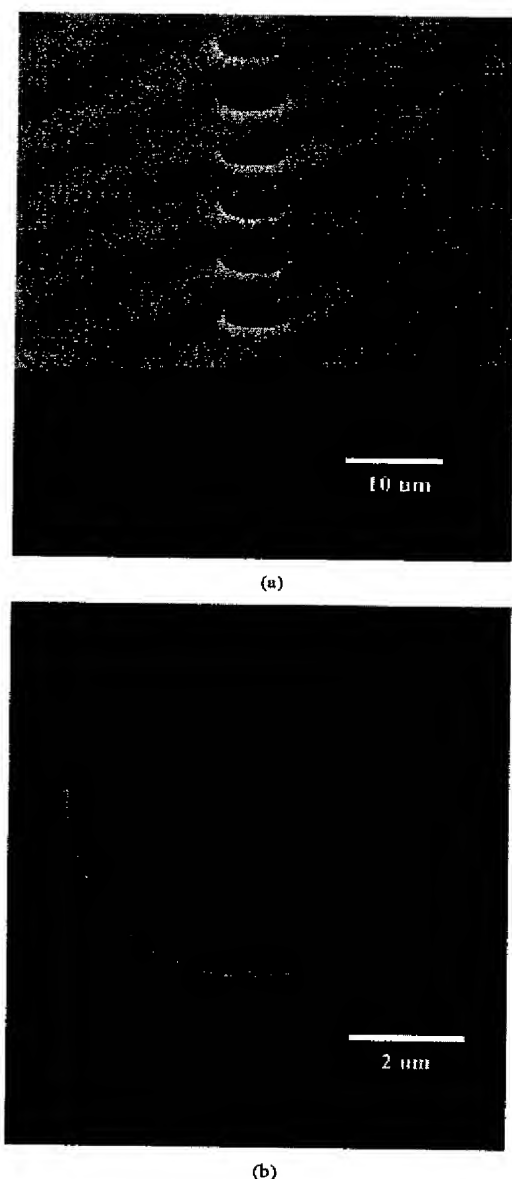
(a)

(b)

Fig. 4. (a) SEM of hemispherical cavities etched into SiO₂. (b) Close-up SEM of cross section of hemispherical cavity. Cavity radius is 3.5 μm.

SIL (step F). The CHF₃ and O₂ flow rates are adjusted to give approximately equal etch rates for the silicon nitride and photoresist [12], enabling the photoresist shape to be transferred to the silicon nitride. Following the plasma etching (CHF₃ : O₂) of the cantilevers (step G), the bulk silicon is plasma etched (SF₆ : C₄F₈) from the backside of the wafer (step H). The cantilevers are released by wet etching the SiO₂ (6 : 1 BOE) and removing the frontside protective layer of photoresist (not shown), with the result as illustrated in step I.

In Step D of Fig. 3, silicon nitride is deposited onto the silicon dioxide surface. Because of the 3–3.5 μm deep hemispherical cavities in the silicon dioxide, the silicon nitride surface after deposition is not flat. Following the deposition of 6.8 μm of silicon nitride on a test wafer, depressions up to several micron

deep in the silicon nitride surface were measured by AFM. If the silicon nitride surface is not planarized, then these depressions are transferred to the tips in the subsequent tip etching process (Step F of Fig. 3). For this reason, the silicon nitride is deposited in two steps (4.1 μm and 2.7 μm), with an intermediate planarization step. After the first step, photoresist is spun on to the wafer to planarize the surface, and the wafer is plasma etched (CHF₃ : O₂). The flow rates of the constituent gases in this etch step are adjusted to give approximately equal etch rates of the silicon nitride and photoresist. This results in the etch planarizing the silicon nitride surface. While resulting surface is not completely flat (illustrated in Step D of Fig. 3), the depressions in the silicon nitride are significantly shallower (<0.35 μm) than without this step (up to several micron), and the resulting tips are therefore free from depressions at the tip apex.

B. Increasing Silicon Nitride Optical Transmission at UV Wavelengths

It is found that increasing the NH₃ flow rate relative to the SiH₄ flow rate improves the transparency of the silicon nitride films at ultraviolet (UV) wavelengths, which in turn improves the optical efficiency of the SIL. This is believed to be due to the increased proportion of NH bonds as compared to SiH bonds (which absorb UV) [13]. The refractive index (n) and absorption (k) measured by spectroscopic ellipsometry [1] are plotted as Fig. 5(a) and (b) as a function of wavelength for a film deposited with the standard NH₃ flow rate and a film deposited with an increased NH₃ flow rate. It is clear that increasing the NH₃ flow rate both lowers the absorption and refractive index at UV wavelengths. This is further evidenced by Fig. 5(c), which shows the optical transmission (measured by a spectrophotometer [2]) through the standard NH₃ flow rate and increased NH₃ flow rate silicon nitride films deposited on quartz substrates. In these measurements, the standard film was 3.5 μm thick and the NH₃ rich film was 6 μm thick. The measurements are of the total transmission through the silicon nitride and quartz substrate and include the effect of absorption in the silicon nitride as well as reflections from the silicon nitride surface. Note that the oscillations in these curves are due to thin film optical interference effects in the silicon nitride film. Clearly, despite the greater thickness of the NH₃ rich film, its optical transmission at wavelengths shorter than 400 nm is considerably higher (78.1%) than the standard film (30.0%). PECVD allows the composition to be varied while maintaining low stress in the film.

IV. SCANNING OPTICAL MICROSCOPE BASED ON MICROMACHINED SIL

A. Experimental Setup

A scanning optical microscope based on the microfabricated SIL is shown as Fig. 6. The microscope operates in both transmission and reflection imaging modes. The light source is a 5 mW gallium nitride (GaN) blue laser diode (λ = 400 nm).[3] The output beam from the laser diode is elliptical, and to make it more circular, the collimation lens is followed by a prism to

[1]SOPRA, Model GESP 6.2, Bois-Colombes, France.
[2]Hitachi, Model U-4001, Japan.
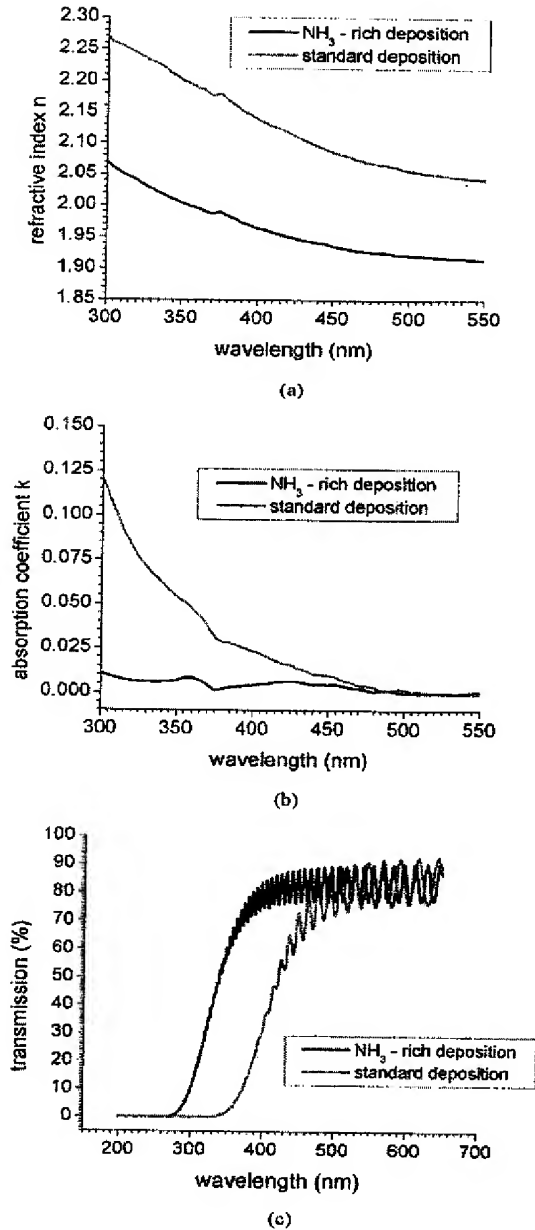[3]Nichia Corporation, Model NLHV500, Tokyo, Japan.

(a)

(b)

(c)

Fig. 5. (a) Real part of refractive index (n) for PECVD silicon nitride films with an NH_3-rich deposition (black curve) and a standard NH_3 deposition (gray curve). (b) Imaginary part of refractive index (k) for PECVD silicon nitride films with an NH_3-rich deposition (black curve) and a standard NH_3 deposition (gray curve). (c) Transmission of thick silicon nitride films deposited on quartz substrates. The NH_3-rich film (black curve) is 6-μm thick and the standard NH_3 deposition (gray curve) is 3.5-μm thick.

compress the beam in its larger dimension. The beam is then reflected by a mirror and passes through a half-wave plate, which rotates the polarization of the beam so that it is transmitted through, rather than reflected by, the polarizing beam splitter that follows it. The beam is then focused by a lens through a pinhole (25 μm diameter) which spatially filters it. The diverging laser beam then passes through a quarter wave plate to convert the polarization of the beam from linear to circular. Following
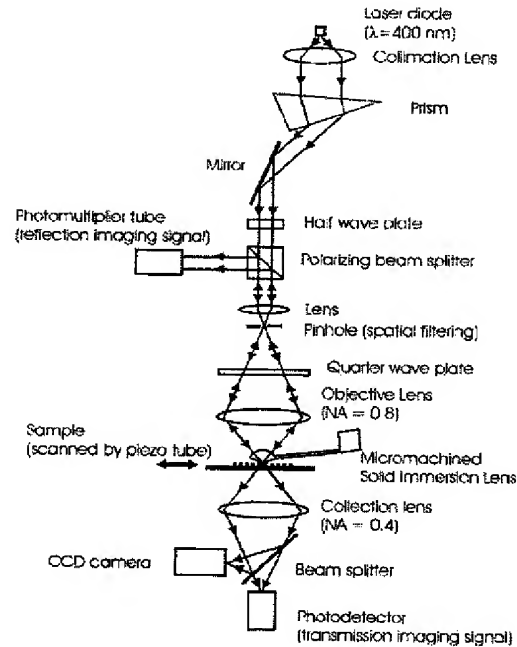

Fig. 6. Solid Immersion Microscope operating in both reflection and transmission imaging modes.

the quarter-wave plate, a high numerical aperture ($NA = 0.8$) microscope lens focuses the laser beam into the SIL to form a spot at the end of the tip. The tip of the SIL is in contact with the sample. Due to the high compliance of the silicon nitride cantilever, the hardness of the sample and the relatively large tip as compared to those used in Atomic Force Microscopy (AFM), closed loop force feedback control is not necessary and tip wear is minimal. Light passing through the SIL and sample is focused by another lens onto a photodetector. Similarly, light reflected from the sample returns through the SIL, through the microscope lens, and passes through the quarter wave plate for a second time, which converts the polarization state from circular back to linear. After passing through the pinhole and lens, the light is reflected by the polarizing beam splitter onto a photomultiplier tube. Because of the quarter-wave plate, the polarization of the light is linear, but 90 degrees to the original state of polarization, so the beam is reflected rather than transmitted by the polarizing beam splitter. The sample is scanned by a piezo-tube and the image of the sample is produced by recording the signals from the photomultiplier tube and photodetector, which measure the reflection and transmission optical signals, respectively. The beam splitter and CCD camera following the collection lens aid in the alignment and focusing of the laser, SIL, and sample.

B. Optical Resolution

The resolution of the SIL microscope is studied by measuring its edge response. The sample used is a titanium grating on a quartz substrate. Fig. 7(a) shows the transmission signal as the sample scans from the metal line (on the left) to the space (on the right). The SIL improves the 20–80% width from 193 nm (without the SIL) to 101 nm (with the SIL), a factor of $\sim$1.91.
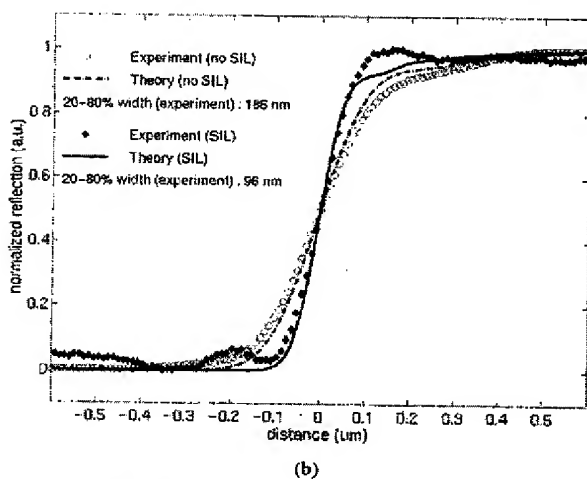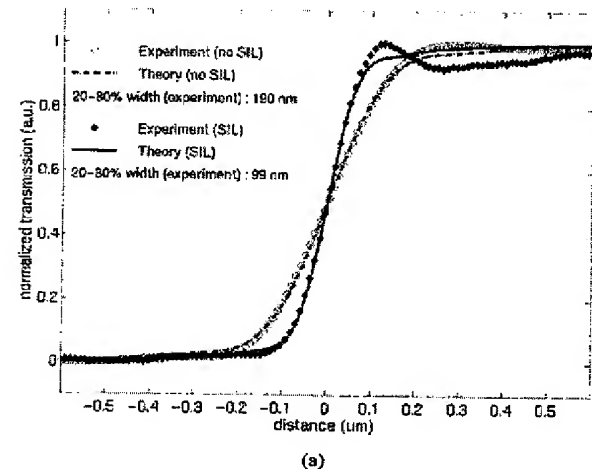
Fig. 7. (a) Edge response (theory and experiment) in transmission as sample is scanned across a titanium line. The SIL improves the edge response by a factor of ~1.91. (b) Edge response in reflection as sample is scanned across a titanium line. As before, the SIL improves the edge response by a factor of ~1.93.
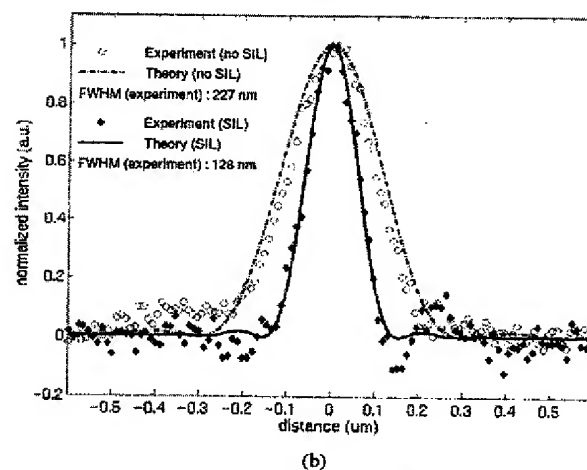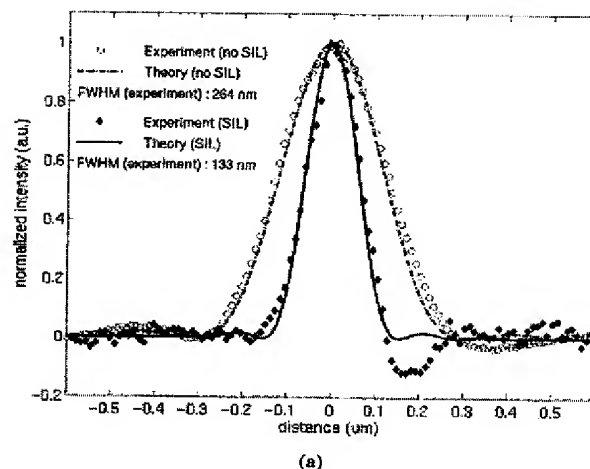

Fig. 8. (a) Point Spread Function (PSF) in transmission mode calculated from the edge response of Fig. 7(a). The SIL improves the FWHM by a factor of ~1.98. (b) Point spread function (PSF) in reflection mode calculated from the edge response of Fig. 7(b). The SIL improves the FWHM by a factor of ~1.77.

The theoretical edge response is also shown, calculated from equation (4) of Section II with the PSF h found by vector diffraction theory and r a step function. For transmission imaging, the theoretical edge response 20–80% width is 180 nm without the SIL and 96 nm with the SIL, a factor of ~1.88 improvement. Fig. 7(b) shows the reflection signal as the sample scans from the space (on the left) to the metal line (on the right). The SIL improves the 20–80% width from 185 nm (without the SIL) to 96 nm (with the SIL), a factor of ~1.93. The theoretical edge response, also shown, has a 20–80% width of 149 nm without the SIL and 81 nm with the SIL, a factor of ~1.84. The theoretical edge response is calculated from equation (2) of Section II.

The theoretical edge response calculated for transmission imaging assumes incoherent illumination. The state of coherence of the laser beam input to the focusing lens is not known exactly, though it may be assumed that it is not perfectly coherent due to the finite coherence length of the laser and the optics used to correct the beam shape. We present the experimental edge response with the theoretical edge response calculated for incoherent illumination because it matches the

experimental data more closely than a coherent calculation. However the experimental edge response displays ringing that is not predicted with incoherent illumination, though it is not as pronounced as would be predicted by a coherent illumination calculation [i.e., Section II, (3)]. Therefore it may be more accurate to consider the illumination as partially coherent.

While the 20–80% edge response widths indicate an improvement in resolution due to the SIL of ~1.9 times, they are sensitive to the ringing in the edge response since this determines the peak value of the edge response. Calculation of the PSF of the system, on the other hand, allows the system resolution to be completely specified. To find the PSF for transmission imaging, the imaging signal is assumed to be of the form of equation (4) of Section II, so that the intensity PSF (h^2) is found by deconvolution of the sample response s^2 (a step function) from the edge response. Fig. 8(a) shows the intensity PSF (h^2) for transmission imaging with and without the SIL, together with the theoretical vector diffraction calculation. The full FWHM spot sizes of Gaussian fits to the data are 264 nm (without the SIL) and 133 nm (with the SIL), a factor of 1.98 improvement. These values compare well with the theoretical spot sizes of

256 nm (without the SIL) and 130 nm (with the SIL). For reflection mode, the imaging signal is assumed to be of the form of equation (2) of Section II. Therefore, to find the PSF h^2, the square root of the imaging signal is taken before deconvolution of the sample response s (a step function). Fig. 8(b) shows the intensity PSF (h^2) for reflection imaging with and without the SIL, together with the theoretical vector diffraction calculation. The FWHM spot sizes of the Gaussian fits are 227 nm (without the SIL) and 128 nm (with the SIL), a factor of 1.77 improvement due to the SIL. These values compare well to the theoretical predictions. That the experimentally measured spot size of ∼130 nm compares well with theory confirms the prediction of Section II that the required dimensional tolerances of the 3.1 μm radius SIL would be met by the micromachining fabrication process.

C. Imaging

To demonstrate the imaging capabilities of the microscope, a titanium grating is imaged. The grating, which was the smallest available to us at the time of the experiment, consists of 0.36 μm wide titanium lines with 0.22 μm wide spaces between the lines. The titanium is 0.1 μm thick and the substrate is quartz. Transmission mode images taken without and with the SIL are shown as Fig. 9(a) and (b) respectively. The dark areas correspond to the titanium lines and the bright areas correspond to the spaces. Because of the smaller spot size that results with the SIL, more light is transmitted through the spaces so that they appear brighter in the image taken with the SIL. This is seen in Fig. 9(c), in which linescans (i.e., single lines of data) from the images of Fig. 9(a) and (b) are shown. The signal measured over the clear area (to the right of the grating) with the SIL is ∼17% of the signal measured without the SIL, for reasons discussed in the following section. However the transmission modulation ratio is improved with the SIL. This is defined to be the ratio of the signal measured over a space to the signal over the clear area with higher values indicating a smaller spot size. The SIL improves the transmission modulation ratio for this grating from 0.58 (without SIL) to 0.87 (with SIL).

Reflection mode images taken without and with the SIL are shown as Fig. 10(a) and (b) respectively. In this case, the bright areas correspond to the titanium lines and the dark areas correspond to the spaces. Because of the smaller spot size that results with the SIL, more light is transmitted through the spaces. Therefore less light is reflected and these spaces appear darker in the image taken with the SIL. This may also be seen from Fig. 10(c), in which linescans from the images of Fig. 10(a) and (b) are shown. The reflection modulation depth is improved by the SIL. This is defined as the ratio of the signal measured over a space (with the signal measured over the clear area subtracted) to the signal over the line (with the signal measured over the clear area again subtracted). A lower value for the reflection modulation depth indicates a smaller optical spot size. The signal measured over the clear area is subtracted as this represents a background signal resulting from reflections from the surface of the SIL. The SIL improves the reflection modulation depth from 0.19 (without SIL) to 0.01 (with SIL). The signal modulation amplitude (i.e., signal measured over the line minus the signal measured over the clear area) with the SIL is ∼58% of the signal modulation measured without the SIL.
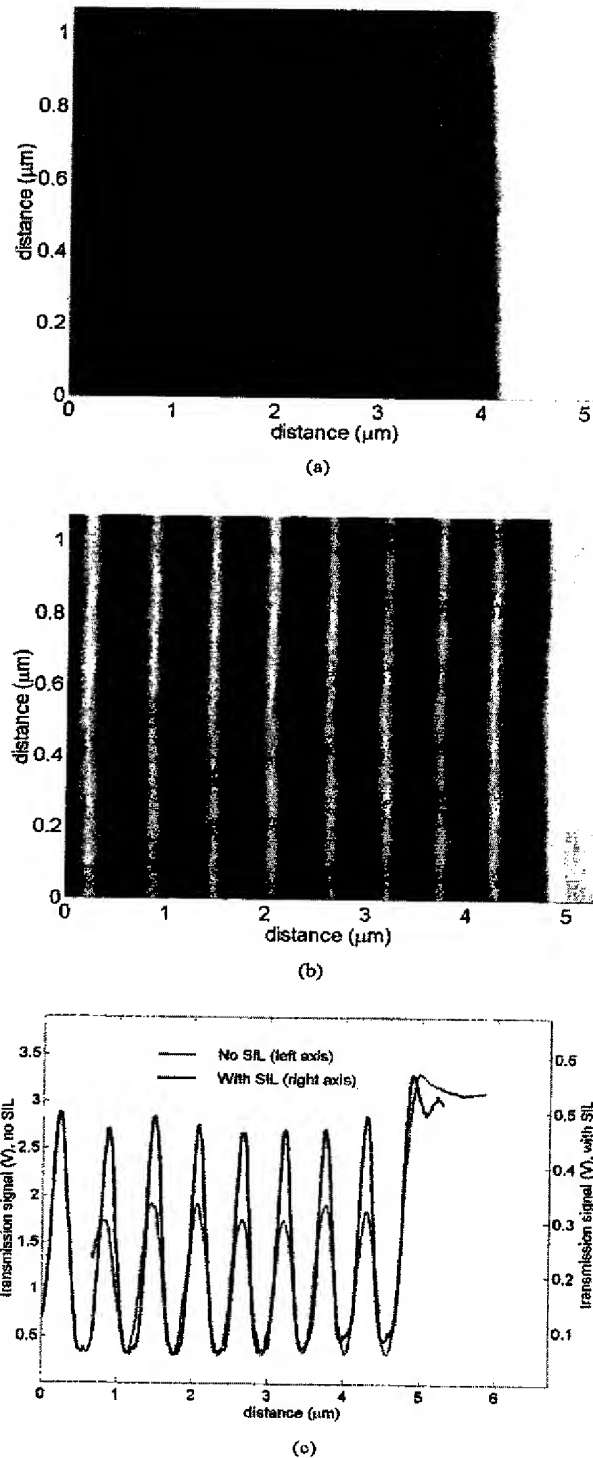

Fig. 9. (a) Transmission mode image of titanium grating, no SIL. (b) Transmission mode image of titanium grating, with SIL. (c) Transmission signal (V) versus distance (μm) with (right axis) and without (left axis) SIL.

D. Optical Transmission Efficiency of SIL

The optical transmission efficiency of the SIL may be calculated from the transmission imaging results shown in Fig. 9.
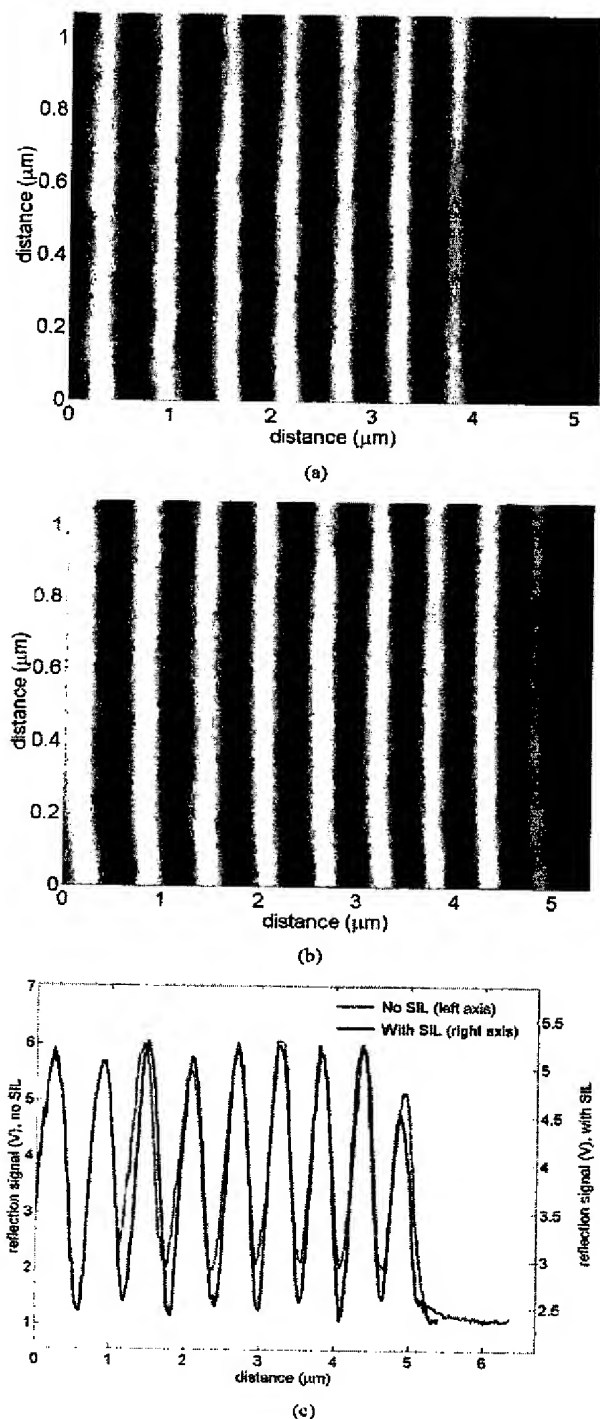
Fig. 10. (a) Reflection mode image of titanium grating, no SIL. (b) Reflection mode image of titanium grating, with SIL. (c) Reflection signal (V) versus distance (μm) with (right axis) and without (left axis) SIL.

In transmission imaging, the signal measured over the clear area with the SIL is ~17% of the signal measured without the SIL. This reduction in optical power is due to increased mismatch of the focusing and collection lens numerical apertures, reflections from the SIL and optical losses in the silicon nitride.

The optical transmission without the SIL is found by taking into account the mismatch between focusing (NA_f 0.8) and collection (NA_c 0.4) lens numerical apertures and the reflections from the sample. Each of the two air–glass ($n_{glass} = 1.46$) interfaces in the sample reflect $R \sim 3.5\%$ of the optical power incident upon them and these reflections may be assumed to add incoherently. Therefore the overall transmission without the SIL is $(1 - R)^2 (NA_c/NA_f)^2 \sim (1 - 0.035)^2 (0.4/0.8)^2 \sim 0.23$. With the SIL, there are reflections of $R_{air-SIL} \sim 10.5\%$ from the air–SIL ($n = 1.96$) interface, $R_{SIL-glass} \sim 2.1\%$ from the SIL–glass interface and $R_{glass-air} \sim 3.5\%$ from the glass–air interface. The focusing numerical aperture is increased to $NA_f = n \sin \theta \sim 1.57$. The expected optical transmission is thus $\sim(1 - R_{air-SIL})(1 - R_{SIL-glass})(1 - R_{glass-air})(NA_c/NA_f)^2 \sim (1 - 0.105)(1 - 0.021)(1 - 0.035)(0.4/1.57)^2 \sim 0.055$. Therefore the optical transmission measured with the SIL is expected to be ~0.055/0.23 ~ 24% of the optical transmission without the SIL. The experimental value of 17% allows us to compute the optical throughput efficiency of the SIL to be ~17/24 ~71%. This is the optical throughput of the SIL with losses are due to scattering from the SIL surface roughness and optical absorption in the silicon nitride.

V. SUMMARY

In this paper, a fabrication method for silicon nitride Solid Immersion Lenses and a microscope based on these lenses have been presented. The surface micromachining method for fabricating the solid immersion lenses uses PECVD silicon nitride, optimized for high optical transmission at UV wavelengths. This fabrication method may also be used with other films (rather than silicon nitride), enabling the solid immersion lenses to be made from a variety of materials (e.g., silicon dioxide for deep-UV wavelengths). Experimental results with the Solid Immersion Microscope based on the micromachined SIL demonstrate an edge response in transmission and reflection of ~100 nm and a spot size of ~130 nm, well below the diffraction limit in air.

REFERENCES

[1] S. M. Mansfield and G. S. Kino, "Solid immersion microscope," *Appl. Phys. Lett.*, vol. 57, pp. 2615–2616, 1990.

[2] E. D. Palik, Ed., *Handbook of Optical Constants of Solids.* New York: Academic, 1985.

[3] E. Betzig and J. K. Trautman, "Near-field optics: Microscopy, spectroscopy, and surface modification beyond the diffraction limit," *Science*, vol. 257, pp. 189–195, 1992.

[4] T. Saiki, S. Mononobe, M. Ohtsu, N. Saito, and J. Kusano, "Tailoring a high-transmission fiber probe for photon scanning tunneling microscope," *Appl. Phys. Lett.*, vol. 68, pp. 2612–2614, 1996.

[5] T. Saiki and K. Matsuda, "Near-field optical fiber optimized for illumination-collection hybrid mode operation," *Appl. Phys. Lett.*, vol. 74, pp. 2773–2775, 1999.

[6] D. A. Fletcher, K. B. Crozier, G. S. Kino, C. F. Quate, K. E. Goodson, D. Simanovskii, and D. V. Palanker, "Near-field infrared imaging with a microfabricated solid immersion lens," *Appl. Phys. Lett.*, vol. 77, pp. 2109–2111, 2000.

[7] D. A. Fletcher, K. B. Crozier, K. W. Guarini, S. C. Minne, G. S. Kino, C. F. Quate, and K. E. Goodson, "Microfabricated silicon solid immersion lens," *J. Microelectromech. Syst.*, vol. 10, pp. 450–459, 2001.

[8] T. R. Corle and G. S. Kino, *Confocal Scanning Optical Microscopy and Related Imaging Systems.* San Diego, CA: Academic Press, 1996.

[9] B. Richards and E. Wolf, "Electromagnetic diffraction in optical systems II. Structure of the image field in an aplanatic system," *Proc. Roy. Soc. A.*, vol. 253, pp. 358–379, 1959.

[10] S. M. Mansfield, "Solid Immersion Microscopy," Ph.D. dissertation, Dep. Appl. Phys., Stanford Univ., CA, 1992.

[11] K. B. Crozier, D. A. Fletcher, G. S. Kino, and C. F. Quate, "Micromachined silicon nitride solid immersion lenses," in *2000 IEEE/LEOS Int. Conf. Optical MEMS*, Kauai, HI, USA, Aug. 21–24, 2000.

[12] H. J. Stocker, "Selective reactive ion etching of silicon nitride on oxide in a multifaceted ('HEX') plasma etching machine," *J. Vac. Sci. Technol. A*, vol. 7, pp. 1145–1149, May/Jun. 1989.

[13] A. Kiermasz and K. Beekman, "Plasma CVD of silicon nitride: Process design for increased flexibility," *Semiconductor Int.*, pp. 108–111, June 1990.

Kenneth B. Crozier (S'01) received the B.Sc. and B.E. degrees (with Honors) in physics and electrical engineering, respectively, from the University of Melbourne, Australia, in 1996. He received the M.S.E.E. degree in electrical engineering from Stanford University, Stanford, CA, in 1999. He is currently pursuing the Ph.D. degree in electrical engineering at Stanford University in the research group of Prof. C. Quate. At Stanford University he has received the Burt and Deedee McMurtry Stanford Graduate Fellowship and the Leland T. Edwards Fellowship.

In 1997, he was employed by the Department of Electrical Engineering at the University of Western Australia. His research interests include micromachining and scanning probe microscopy.

Daniel A. Fletcher received the B.S.E. degree in mechanical and aerospace engineering *summa cum laude* from Princeton University, Princeton, NJ, in 1994 and the D.Phil. degree in engineering science from the University of Oxford, U.K., in 1997, where he was a Rhodes Scholar. He received the Ph.D. degree in mechanical engineering from Stanford University in 2001 as a National Science Foundation Graduate Research Fellow.

He was a Postdoctoral Researcher at Stanford University, Stanford, CA. He joined the University of California, Berkeley, as an Assistant Professor in the Bioengineering Department, where he uses micromachined devices for high-resolution optical and force microscopy of cells.

Gordon S. Kino (S'52–A'54–SM'63–F'66–LF'94) received the B.Sc. and M.Sc. degrees in mathematics from the London University, U.K., and the Ph.D. degree in electrical engineering at Stanford University, Stanford, CA.

He is the W. M. Keck Foundation Professor of Electrical Engineering, Emeritus, and Professor (by courtesy) of Applied Physics, Emeritus. He was the Director of the Ginzton Laboratory at Stanford University. He has worked on microwave tubes, electron guns, plasmas, the Gunn effect, acoustic devices, acoustic imaging, nondestructive testing, fiber-optics, and microscopy. His current interests are in various forms of microscopy, acoustic devices, fiber optics, and optical storage. He has published over 430 papers and 47 patents. He and his students have developed new types of scanning optical microscopes and interferometric microscopes. He and T. Corle are the authors of *Confocal Optical Microscopy and Related Techniques* (New York: Academic, 1996), and he is the author of *Acoustic Waves: Devices, Imaging, and Analog Signal Processing* (Englewood Cliffs, NJ, Prentice-Hall 1987).

Dr. Kino was a Guggenheim Fellow in 1967. He is a Fellow of the American Physical Society and the AAAS, and a Member of the National Academy of Engineering. In 1984, he received the IEEE Sonics and Ultrasonics Group Achievement Award and in 1986 the ASNT Achievement Award in Applied Research.

Calvin F. Quate (S'43–A'50–M'55–F'65–LF'89) is the Leland T. Edwards Professor of Electrical Engineering at Stanford University. His research focuses on the development and application of scanning probe microscopes.